Journal of Rock Mechanics and Geotechnical Engineering 9 (2017) 210–225

Contents lists available at ScienceDirect

Journal of Rock Mechanics and Geotechnical Engineering

journal homepage: www.rockgeotech.org

Full Length Article

Risk of shear failure and extensional failure around over-stressed excavations in brittle rock

Nick Barton [a,*], Baotang Shen [b]

[a] Nick Barton & Associates, Oslo, Norway
[b] CSIRO Energy, Brisbane, Australia

ARTICLE INFO

Article history:
Received 13 June 2016
Received in revised form
10 November 2016
Accepted 14 November 2016
Available online 30 November 2016

Keywords:
Fracture propagation
Tension
Shear
Poisson's ratio
Break-out
Rock burst
Deep tunnels
FRACOD model

ABSTRACT

The authors investigate the failure modes surrounding over-stressed tunnels in rock. Three lines of investigation are employed: failure in over-stressed three-dimensional (3D) models of tunnels bored under 3D stress, failure modes in two-dimensional (2D) numerical simulations of 1000 m and 2000 m deep tunnels using FRACOD, both in intact rock and in rock masses with one or two joint sets, and finally, observations in TBM (tunnel boring machine) tunnels in hard and medium hard massive rocks. The reason for 'stress-induced' failure to initiate, when the assumed maximum tangential stress is approximately (0.4–0.5)σ_c (UCS, uniaxial compressive strength) in massive rock, is now known to be due to exceedance of a critical extensional strain which is generated by a Poisson's ratio effect. However, because similar 'stress/strength' failure limits are found in mining, nuclear waste research excavations, and deep road tunnels in Norway, one is easily misled into thinking of compressive stress induced failure. Because of this, the empirical SRF (stress reduction factor in the Q-system) is set to accelerate as the estimated ratio $\sigma_{\theta\max}/\sigma_c >> 0.4$. In mining, similar 'stress/strength' ratios are used to suggest depth of break-out. The reality behind the fracture initiation stress/strength ratio of '0.4' is actually because of combinations of familiar tensile and compressive strength ratios (such as 10) with Poisson's ratio (say 0.25). We exceed the extensional strain limits and start to see acoustic emission (AE) when tangential stress $\sigma_\theta \approx 0.4\sigma_c$, due to simple arithmetic. The combination of 2D theoretical FRACOD models and actual tunnelling suggests frequent initiation of failure by 'stable' extensional strain fracturing, but propagation in 'unstable' and therefore dynamic shearing. In the case of very deep tunnels (and 3D physical simulations), compressive stresses may be too high for extensional strain fracturing, and shearing will dominate, both ahead of the face and following the face. When shallower, the concept of 'extensional strain initiation but propagation' in shear is suggested. The various failure modes are richly illustrated, and the inability of conventional continuum modelling is emphasized, unless cohesion weakening and friction mobilization at different strain levels are used to reach a pseudo state of yield, but still considering a continuum.

© 2017 Institute of Rock and Soil Mechanics, Chinese Academy of Sciences. Production and hosting by Elsevier B.V. This is an open access article under the CC BY-NC-ND license (http://creativecommons.org/licenses/by-nc-nd/4.0/).

1. Introduction

We will start by illustrating two very different failure modes, both of them being 'physical realities' but from very different environments. The first is from petroleum well-bore simulations in sandstones. With change of scale, a small deep tunnel in a weak but brittle rock can be envisaged. Failure is dominated by (log-spiral) shearing (Fig. 1). The second is a real case involving highly-stressed granite in an underground research laboratory (URL): the URL in Canada. Crack initiation is induced by tensile/extensional fracturing, but there is shearing, buckling, and a final characteristic notch (see Fig. 2). In the following investigations, both tensile (or extensional strain) initiation and progression in shear have their important roles to play. Tensile initiation may consist of critical strain-initiated extensional fracturing, which can explain several puzzling phenomena such as tensile fracturing in entirely compressive stress fields (e.g. Fairhurst and Cook, 1966).

* Corresponding author.
E-mail address: nickrbarton@hotmail.com (N. Barton).
Peer review under responsibility of Institute of Rock and Soil Mechanics, Chinese Academy of Sciences.

http://dx.doi.org/10.1016/j.jrmge.2016.11.004
1674-7755 © 2017 Institute of Rock and Soil Mechanics, Chinese Academy of Sciences. Production and hosting by Elsevier B.V. This is an open access article under the CC BY-NC-ND license (http://creativecommons.org/licenses/by-nc-nd/4.0/).

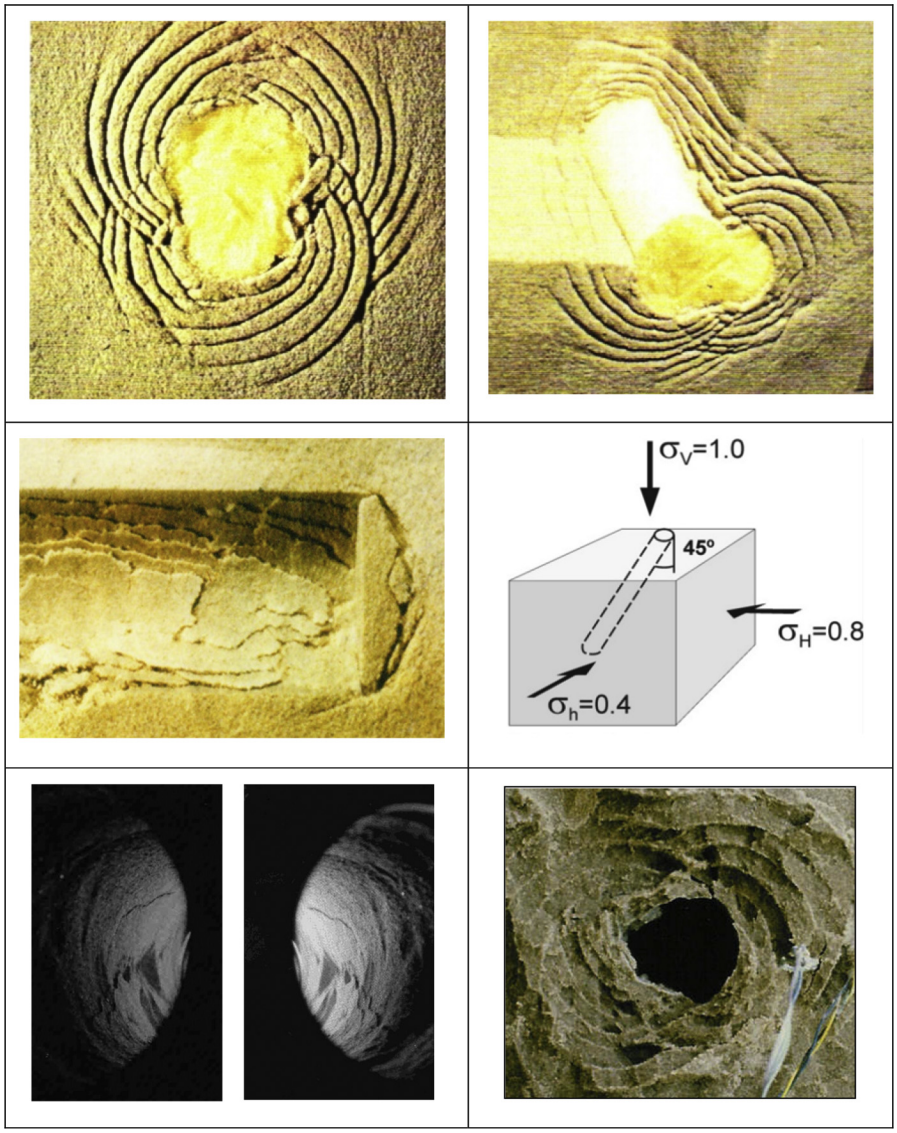

Fig. 1. Obvious log-spiral shearing in model tunnels/well-bores, which were drilled into highly-stressed blocks (measuring 0.5 m × 0.5 m × 0.5 m) of weak model sandstone. All three principal stresses could be varied independently through flat-jack loading, and drilling did not need to be parallel to any of the principal boundary stresses. (Flat-jacks could have central or off-centre holes). The upper four photographs show the results of stress anisotropy and hole deviation from the horizontal. The lower two photographs show tests in a smaller polyaxial cell in which hole drilling was parallel to the minimum horizontal stress. Miniature monitoring boreholes and pressure cells were installed before drilling under 3D stress. Coloured cemented sand in the pre-drilled boreholes (an idea from Dr. Stavros Bandis) confirmed that 'log-spiral' shearing does indeed involve discrete, repeated, log-spiral shear displacements, somewhat different from the 'zonal disintegration' phenomena described and modelled by Wu et al. (2008). Tensile/extensional modes were not evident in these physical model studies, which might be due to the level of confinement. From the first author's joint-industry petroleum-sponsored project at NGI, 1986–1988. See some of our published results in Addis et al. (1990).

2. Stress-strength ratio introduction

Forty years ago, when the Q-system of Barton et al. (1974) was developed, 'stress-induced' fracturing was assumed to initiate when the ratios of UCS/major principal stress (or σ_c/σ_1 in Table 1) became <5, or the inverse >0.2. The recommended value of SRF (stress reduction factor) was increased rapidly, so as to make tunnel support adequate, since high SRF values ensured heavier support in the case of newly fractured massive rock. As many more high-stress case records were collected between 1987 and 1993 by former NGI (Norwegian Geotechnical Institute) geologist and tunnelling colleague Eystein Grimstad, mostly from deep Norwegian road tunnels, where 'stress-fracturing' and rock bursting had been experienced, we added the second column seen in the lower table in Table 1 (σ_θ/σ_c). An appendix in Barton and Grimstad (2014) records the details of these historic (pre-1990s) case records. A number of ratios of σ_θ/σ_c were in the range 0.4–0.8, with a maximum value of 1.2 at Strynefjell. The depth range was between 600 m and 1400 m.

As can be noted from the second tabulation in Table 1, from Grimstad and Barton (1993), an acceleration of SFR values is noted when the ratio σ_θ/σ_c increases above 0.4, with sharp acceleration when 0.5 is exceeded and 'moderate slabbing', 'rock burst' and 'strain burst' are recorded, needing rapidly increasing SRF. There are additional comments on 'strain bursting,' 'rock slabbing' and 'block yielding' for given depths and Q-value ranges in Barton and Grimstad (1994), using Singh et al. (1992) suggestions for relating the Q-value to an estimate of the strength of the rock mass. This

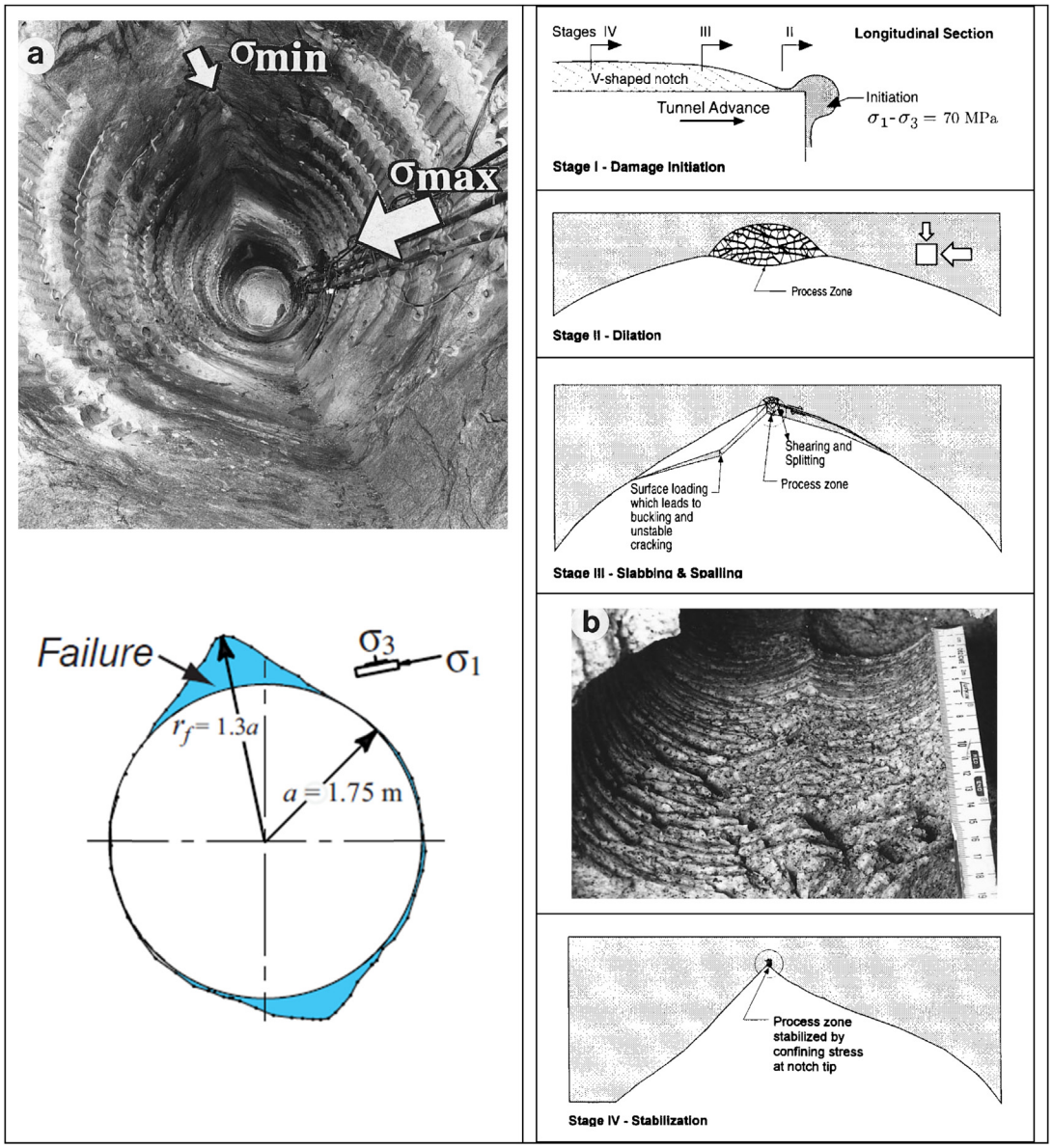

Fig. 2. The careful observations of cracking initiation and propagation at the URL site in Manitoba, Canada where Atomic Energy Canada Limited (AECL) researchers conducted a very gradual excavation by line-drilling so as to be able to observe the processes as closely as possible. Tunnel-face-corner initiation in the third dimension was suspected, followed by (extensional) splitting, shearing and buckling. Adapted from Read and Martin (1996) and Martin (1997), with some of the detailed text removed for clarity of reproduction.

was suggested as $7\gamma Q^{1/3}$ (MPa). In Barton (2000), $\sigma_c = 5\gamma Q_c^{1/3}$ (MPa) is preferred for estimation with TBM, in comparison with cutter force (e.g. rock density $\gamma = 2.6$ t/m^3).

It is of interest to note that Martin et al. (1999) found, independently of our earlier descriptions of (assumed) stress-induced failure from 1974 to 1993 Q-system publications, that in mining excavations (mostly collected from others), and from Canadian nuclear waste (URL) research, there was a well-documented expectation of (assumed) stress-induced failure initiating when the maximum tangential stress/strength ratio reached about 0.4–0.5. This is shown in Fig. 3. When first seen by the first author about 15 years ago, this was an encouraging 'support' for what we had been observing for a long time in deep Norwegian tunnels, and had been empirically absorbed in the Q-system, in order to estimate appropriate SRF values. More recently in Grimstad and Barton (1993), we were addressing the case of exceptionally massive rock (see Table 1 descriptions) which 'facilitated' rock bursts when depth was sufficient.

Martin et al. (1999) quoted the following equation for describing the best fit line, as indicated in Fig. 3 (Note that $\sigma_{max} = 3\sigma_1 - \sigma_3$ in Eq. (1)).

$$R_f/a = 0.49(\pm 0.1) + 1.25\sigma_{max}/\sigma_c \quad (1)$$

where R_f and a are defined in the inset of Fig. 3; σ_1 and σ_3 are the maximum and minimum principal stresses, respectively. As seen in Fig. 3, failure initiates when $\sigma_{max}/\sigma_c \approx 0.4 \pm 0.1$, in the same stress/strength region as in the Q-system 'acceleration' of SRF (see Table 1). The interesting thing about all this similarity is that it is for entirely different, critical extensional-strain related reasons, in which familiar ratios of σ_c/σ_t and familiar magnitudes of Poisson's ratio 'cancel-out' to produce this most frequently occurring stress/strength ratio of 0.4. We have been deceived for decades by continuing to think conventionally along the lines of continuum strength criteria, as opposed to discontinuous failure criteria. See

Table 1
The Q-system based estimation of appropriate SRF (stress reduction factors) from Barton et al. (1974) (top) and Grimstad and Barton (1993) (bottom). Hoek and Brown (1980) used the inverse (σ_1/σ_c) to categorize failure of square openings from South Africa. Note that the third column of numbers is SRF in each case. Grimstad and Barton's (1993) paper was mainly a Q-system tunnel and cavern support-method update from $S(mr)$ to $S(fr)$. We expanded the SRF estimation in the case of exceptionally massive rock with risk of rock burst, to include the ratio of (estimated) maximum tangential stress σ_θ/σ_c using the laboratory-scale value of UCS for σ_c. From 1993, we ceased to use the ratio σ_t/σ_1 (σ_t is the tensile strength). This was perhaps unwise in view of what is to follow concerning extensional-strain fracture initiation.

(a) Competent rock, rock stress problems		σ_c/σ_1	σ_t/σ_1	SRF	Note: This table is an extract of Barton et al. (1974). In some mining circles (Western Australia) where high stress occurs with deep-level jointing, categories L and M are still used, in preference to the (three) updated SRF values from Grimstad and Barton (1993).
H	Low stress, near surface	>200	>13	2.5	(ii) For strongly anisotropic stress field (if measured) when 5 $\leq\sigma_1/\sigma_3 \leq 10$, reduce σ_c and σ_t to $0.8\sigma_c$ and $0.8\sigma_t$; when $\sigma_1/\sigma_3 > 10$, reduce σ_c and σ_t to $0.6\sigma_c$ and $0.6\sigma_t$ where: σ_c = unconfined compression strength, σ_t = tensile strength (point load), σ_1 and σ_3 = major and minor principal stresses
J	Medium stress	200–10	13–0.66	1.0	
K	High stress, very tight structure (Usually favourable to stability, may be unfavourable to wall stability)	10–5	0.66–0.33	0.5–2.0	
L	Mild rock burst (massive rock)	5–2.5	0.33–0.16	5–10	
M	Heavy rock burst (massive rock)	<2.5	<0.16	10–20	
(b) Competent rock, rock stress problems		σ_c/σ_1	σ_θ/σ_c	SRF	Note: This Grimstad and Barton (1993) update of three SRF values for massive, unjointed rock masses, also includes the column σ_θ/σ_c, which is estimated from elastic theory: $\sigma_{\theta\ \max} = 3\sigma_1 - \sigma_3$
H	Low stress, near surface, open joints	>200	<0.01	2.5	
J	Medium stress, favourable stress condition	200–10	0.01–0.3	1	
K	High stress, very tight structure. Usually favourable to stability, may be unfavourable for wall stability	10–5	0.3–0.4	0.5–2	
L	Moderate slabbing after >1 h in massive rock	5–3	0.5–0.65	5–50	
M	Slabbing and rock burst after a few minutes in massive rock	3–2	0.65–1	50–200	
N	Heavy rock burst (strain-burst) and immediate dynamic deformations in massive rock	<2	>1	200–400	

discussion in Barton (2003). Fig. 3 and our SRF estimation in the Q-system make the assumption that compressive strength is directly involved, together with continuum-based Kirsch-related compressive tangential stresses.

3. Stress-strength ratios suggesting failure, explained by other means

Brace (1964), Gramberg (1965), Fairhurst and Cook (1966), and Brown and Trollope (1967) are among the very first to have pointed out the importance of axial splitting in response to compressive stress fields, when neighbouring surfaces are available to allow the 'lateral' extensional strain to cause extensional fracturing. Somewhat later, Stacey (1981) used extensional-strain theory in an attempt to predict brittle failure mechanisms in deep massive quartzites in South Africa. He showed that for a material that shows linear deformation behaviour, the onset of failure and the depth of failure could be related to a consideration of extensional strain. A 3D equation for expressing extensional strain (in the lateral direction) is as follows:

$$\varepsilon_3 = \frac{1}{E}[\sigma_3 - \nu(\sigma_1 + \sigma_2)] \tag{2}$$

where ν is the Poisson's ratio of the intact rock and E is the Young's modulus. He proposed that if the calculated extensional strain was greater than the critical strain, then spalling would occur. So if $\nu(\sigma_1 + \sigma_2) > \sigma_3$, then (negative) extensional strain will occur. Stacey (1981) listed numerous critical extensional strains for a variety of rock types, based on laboratory compression tests. Mostly, critical strains in the lateral direction were close to 0.0001. These strains correspond to a stress level of about 30% of UCS, which we can see from a sophisticated set of laboratory test recordings from Martin (1997), correspond approximately with Fig. 4 (Canadian granite results).

The present two authors considered a closely related approach. We use both extensional strain and tensile strength as the criterion for fracture initiation, even when all stresses are positive (compressive). We do not focus here on cohesion loss and friction mobilization at different strains, as some other researchers, although support this approach if performing continuum modelling (as for instance by Hajiabdolmajid et al. (2000) and Barton and Pandey (2011)). Careful laboratory testing reported by Martin and Chandler (1994) demonstrates that cohesion is lost and friction is mobilized at different levels of strain. This is equivalent to Müller (1966) observations at *rock mass* scale, that when intact bridges (cohesion) are broken 'friction remains'. So at both scales we cannot add 'c' and '$\sigma_n \tan\varphi$' when performing continuum modelling, but must disassociate and consider 'c' *then* '$\sigma_n \tan\varphi$', or CC *then* FC when using Q-value derived parameters (Barton, 2002). However, in the following FRACOD fracture mechanics modelling (Shen et al., 2013), a discontinuum approach is used both to generate (if relevant) and to propagate the extensional fracturing, most frequently in shearing mode. The important and very well-known principle is that although the rock may be under compression (around a highly stressed excavation), tensile strain may exist in the nearly unloaded direction (i.e. radial direction) perpendicular to the major compressive (tangential) stress, due to Poisson's effect. Considering just the 2D case, we can write:

$$\varepsilon_x = \frac{1}{E'}(\sigma_x - \nu\sigma_y) \text{ or } \varepsilon_{\text{radial}} = \frac{1}{E'}\left(\sigma_{\text{radial}} - \nu\sigma_{\text{tangential}}\right) \tag{3}$$

where ε_x is the elastic strain in the x-direction (i.e. radial). E' is the equivalent Young's modulus ($E' = E$ for plane stress condition; $E' = E/(1-\nu^2)$ for plane strain condition). The radial strain ε_x can be

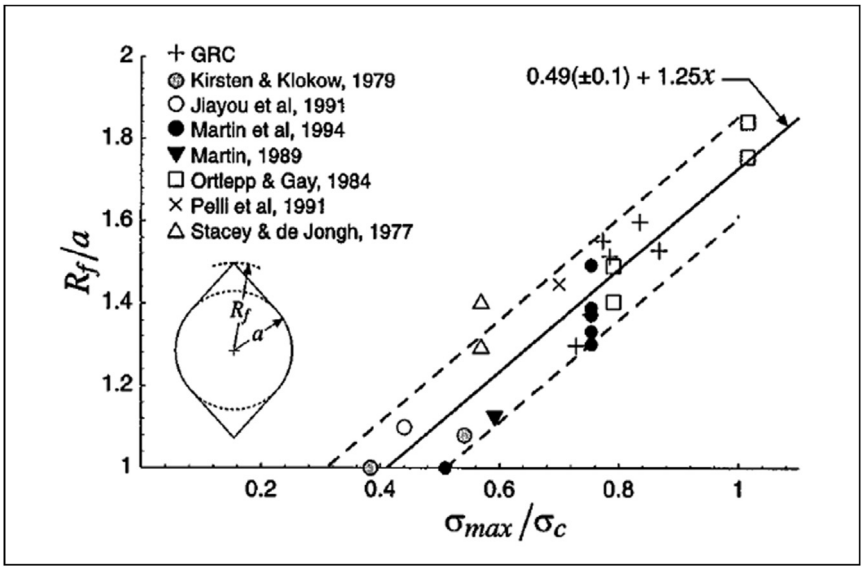

Fig. 3. Observations of failure initiation and depth of 'stress-induced' over-break, from Martin et al. (1999). These authors did not seem to be aware that the Q-system had independently come to the same stress/strength ratio some years earlier, using deep road tunnels in Norway (and deep hydropower tunnels in China and Chile) as the source of case records. In fact, as we shall see, the common stress/strength ratios of 0.3, 0.4, or 0.5 occur for other reasons: due to extensional strain fracturing and some simple arithmetic concerning typical ratios of σ_c/σ_t (about 10) and Poisson's ratio (about 0.25). For references of the data points given in this figure please refer to Martin et al. (1999).

extensional (negative) even if both σ_x and σ_y are compressive stresses. When ε_x reaches the critical strain ε_c ($\varepsilon_c = -\sigma_t/E'$), it is considered that tensile fracture initiation will occur, on a small-scale at first, with possible coalescence and (unstable) more widespread shear failure following, if tangential stress levels are high enough.

Extensional (i.e. tensile failure) fracturing will occur in the radial (unloaded) $\sigma_y \approx 0$ direction when the stress σ_y (i.e. $\sigma_{\text{tangential}}$) meets the condition given in Eqs. (4) and (5).

$$-\frac{\sigma_t}{E'} = \varepsilon_c = -\frac{\nu\sigma_y}{E'} \text{ or } -\frac{\sigma_t}{E'} = \varepsilon_c = -\frac{\nu\sigma_{\text{tangential}}}{E'} \tag{4}$$

Cancelling E' yields:

$$\sigma_y = \frac{\sigma_t}{\nu} \text{ or } \sigma_{\text{tangential}} = \frac{\sigma_t}{\nu} \tag{5}$$

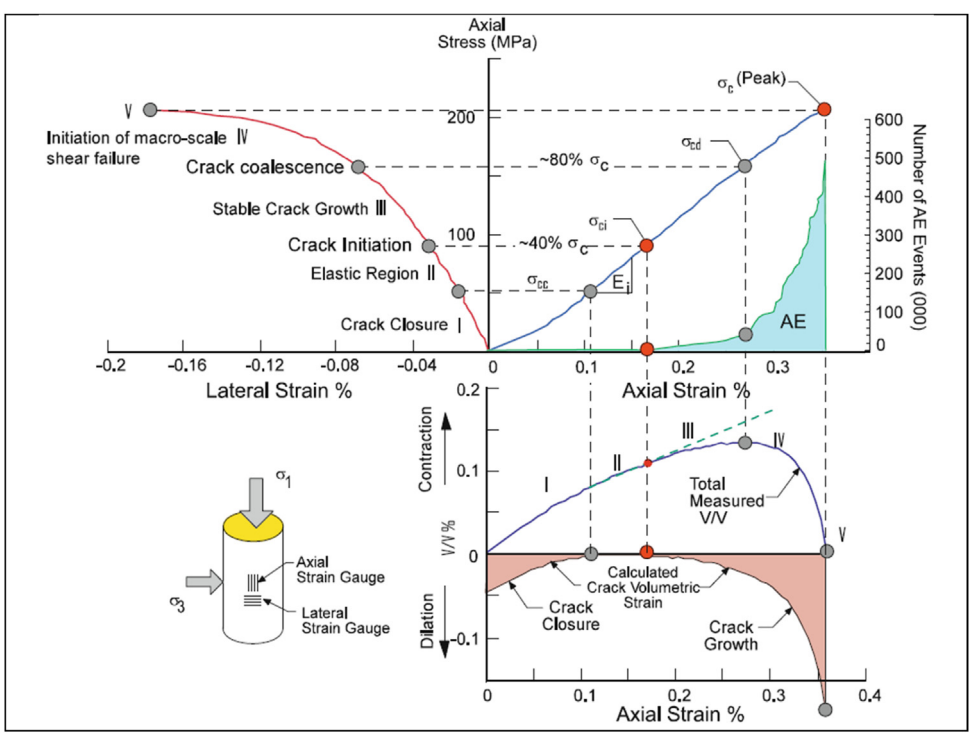

Fig. 4. Martin (1997) presented this comprehensive laboratory test result showing brittle failure phenomena for Lac du Bonnet granite from the Underground Research Laboratory (URL). Crack initiation and acoustic emission occur at about 40% of the peak value of σ_c. Note lateral strains approaching 0.0016 (higher than that in Stacey (1981)).

For rocks with the UCS about 10 times the tensile strength (σ_t) and Poisson's ratio $\nu = 0.25$, the expected *tangential compression stress* level for extensional (tension-failure) fracturing in the radial direction is as follows from simple arithmetic. Second author Dr. B. Shen was adding a sub-routine to FRACOD when he noticed the following:

$$\sigma_{\text{tangential}} = \sigma_y = \frac{UCS}{10\nu} = \frac{UCS}{10 \times 0.25} = 0.4UCS \tag{6}$$

Hence the frequent occurrence of ratio 0.4 ($\pm$0.1) for $\sigma_{\text{tangential}}/UCS$ when spalling commences, with the related need for much

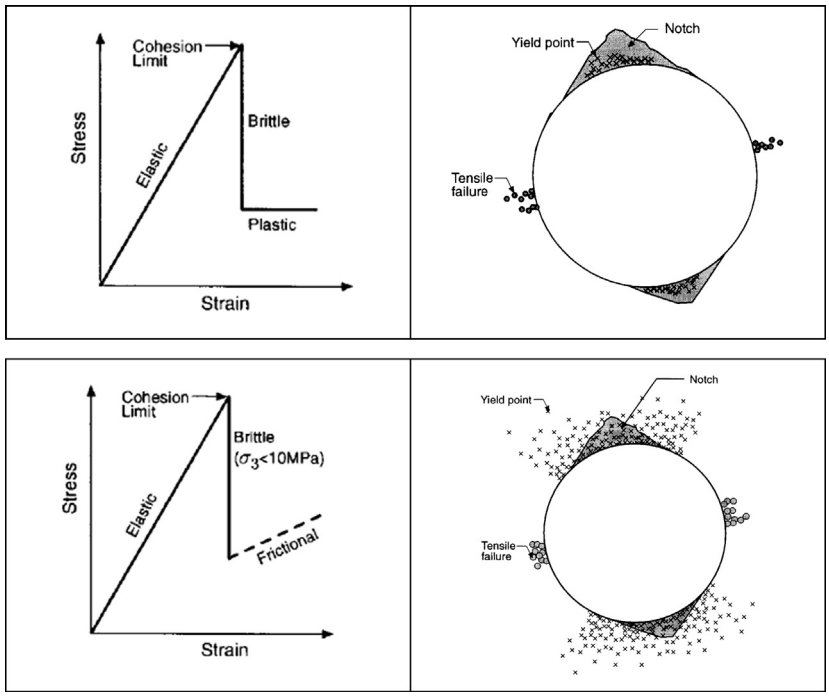

Fig. 5. Continuum modelling of the URL break-out as reported by Martin (1997) using the popular finite element programme marketed by Rocscience: PHASES. The predictions of 'yield' (*x*-points) have only partial relevance to the reality, and of course being a continuum, no actual fracturing (or break-out) occurs.

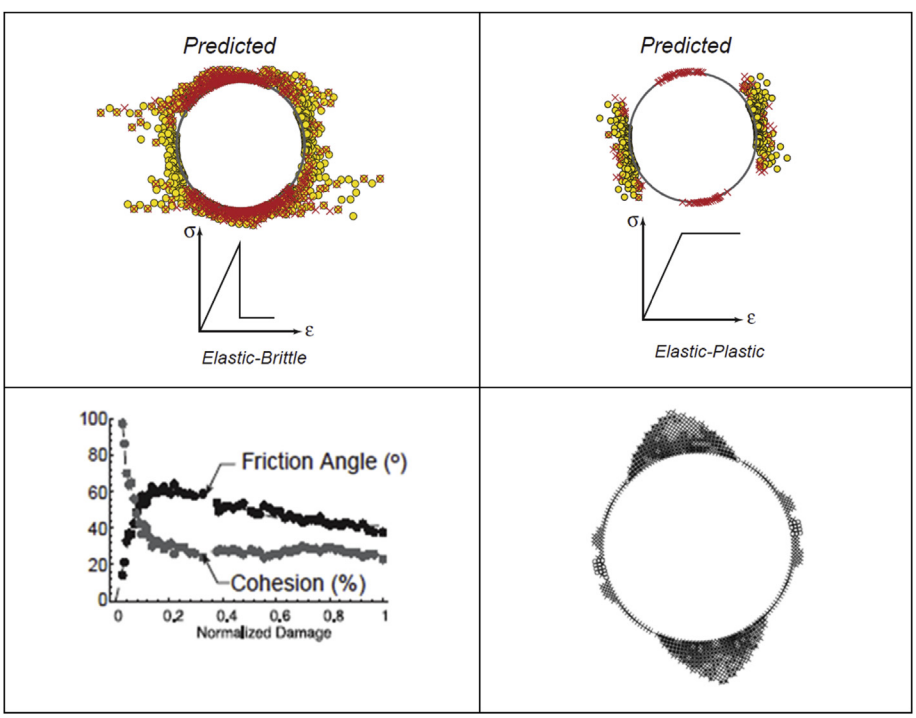

Fig. 6. Continuum modelling of the URL break-out. Partial success is demonstrated with degradation of cohesion and mobilization of friction as performed with FLAC (bottom-left). Application of conventional Mohr-Coulomb (or nonlinear Hoek-Brown) with PHASES was shown to be very unrealistic. This modelling was described by Hajiabdolmajid et al. (2000), with well-known co-authors Martin and Kaiser.

higher SRF when utilizing the Q-system to select single-shell (NMT, Norwegian Method of Tunnelling) tunnel support. The ratio 0.4 is seen to be typical in laboratory tests as well (Fig. 4). Crack initiation and AE (acoustic emission) start for an entirely logical failure-mechanism reason, as opposed to failure-criterion reason (a subtly differentiated goal mentioned by Bieniawski (1967)).

4. Limitations of continuum modelling

Numerous authors during the last decades have pointed out the limitations of conventional continuum modelling for predicting the onset of (extensional) spalling surrounding over-stressed tunnels, shafts or raises, whether excavated by drill-and-blast and TBM (or even by line drilling) methods. Mohr-Coulomb and more recently the non-linear (though not sufficiently nonlinear) Hoek-Brown strength criteria for linear-elastic continua, may often 'miss' the onset of spalling by a wide margin, when modelling shear failure in highly compressive *stress* conditions. Stacey (1981) referred to the early onset of tunnel-face fracturing ahead of a TBM used in a deep gold mine, with difficulties due to the rotation of this large 'disk' of rock ahead of the cutters. Such phenomena were also experienced in the deep-base rail tunnels under the Alps. Stacey and Yathavan (2003) referred to the moderate levels of major principal stress (σ_1) recorded by Grimstad in deep road tunnels in Norway: typical range: 0.1–

Table 2
Failure modes typical of tunnels and well-bores (Barton, 2003).

Description	Mode of behaviour
1. Hard, massive, brittle rocks that dilate during failure even when stresses are high. Stress-induced failure may be delayed as 'strength corrosion' occurs	1. Extension failure, thin-walled stress-slabbing, dynamic ejection, bursting. The symmetric 'dog-eared' fallout due to the anisotropic stresses may have a 'nose'. Deformations can be large
2. Hard or medium hard, bedded and jointed rock that can shear and dilate along structural planes, while under moderate to high stress levels	2. Anisotropic response. Shear stress dissipates by slight shear on bedding planes and joints. Deformations are moderate. Block falls can occur
3. Soft, massive, non-brittle rocks that may, or may not dilate during shear failure. Typical for young (e.g. Tertiary) rocks such as the mudstones and siltstones in Japan	3. Failure may occur by log-spiral shear development and tangential strain. Radial deformations are large, and pressure on support is high. (Twin tunnels need pillars 4 to 5 times their span c.f. Japan, Taiwan (China))
4. Very soft, plastic rocks (and clays) that contract when sheared under significant stress levels	4. Post-peak strength loss reaches an extreme of virtual 'flow', and tunnel closure can occur

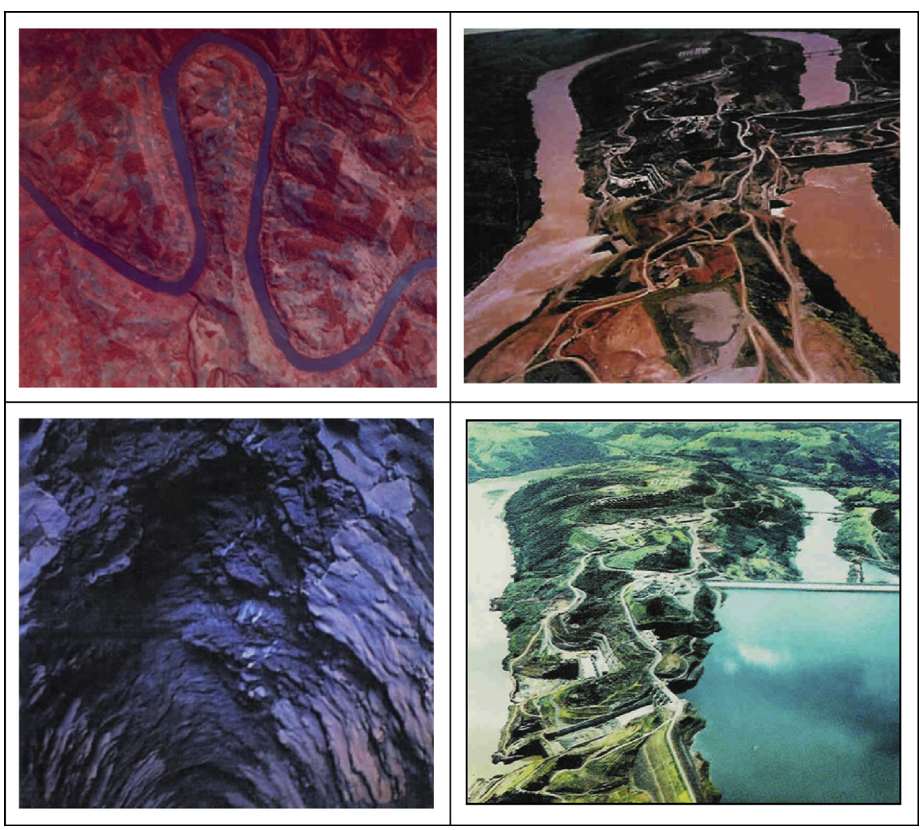

Fig. 7. The 125 m Itá CFRD dam, reservoir and 1450 MW power plant in Brazil. The satellite photo shows a distinctive NNW-oriented 11 km loop in the Uruguay River, and a distinctive ridge (and igneous dyke) with the same NNW orientation. We can surmise that this (>5 km long) dyke was also formed by extensional strain mechanisms. The power plant was located across the narrow 1 km ridge. All tunnels crossing this ridge (five diversion and flood-control tunnels of 15 m × 17 m and 14 m × 16 m dimensions, and five 9 m diameter, 53° inclined pressure tunnels) suffered stress-induced (or extensional-strain-induced) fracturing during construction, with 2 m–3 m deep break-out in the arch and more in the invert due to erosion effects.

0.4 for the ratio σ_1/σ_c, yet spalling or even bursting was recorded in each of the thirteen cases. See Barton and Grimstad (2014).

The two different approaches illustrated in Fig. 5, from two of Martin's (1997) analyses of the URL break-out (shown in Fig. 2), utilize a Mohr-Coulomb style of linearity, with distinct elastic-brittle-plastic or the less conventional elastic-brittle-frictional mobilization. The latter implies not only loss of cohesion, but also subsequent mobilization of friction. Yield points seem either to be too conservative or too liberal in relation to the reality. The conventional and an unconventional solution to modelling the URL break-out as shown in Fig. 6 demonstrates the dilemma of continuum modellers rather clearly, because although equipped with Mohr-Coulomb or Hoek-Brown 'shear strength criteria', they are not in any significant way 'failure criteria' for intact brittle rock. Therefore they fail to model the mechanisms of the 'main event': extensional-strain fracturing followed by discontinuous propagation in shearing, if stress levels are high enough. As we shall see FRACOD does a much more realistic job.

The degradation of cohesion and mobilization of friction utilized by Hajiabdolmajid et al. (2000) and its implementation in FLAC seem to work well in terms of mirroring the failed zone (Fig. 6) even if not always for the right reasons. The limitations of continuum modelling have been discussed further in Barton (2003) and contrasted to the wide ranges of behaviour found in the real world of tunnelling. A table reproduced from this discussion is shown in Table 2.

5. Some observations of failure or heavy over-break in tunnels

The first case is a highly stressed series of hydropower tunnels, despite their relatively near-surface location. With depths of over-break shown in Fig. 7 in the range 2 m–3 m for an average tunnel 'radius' of about 8 m, we see from Fig. 3 (Martin et al., 1999) that ratios of σ_{max}/σ_c of about 0.6–0.7 are implied when R_f/a is in the range of (8 + 2 or 3 m)/8 = 1.25 to 1.38. Taking σ_c as an average 200 MPa, the above implies that the maximum tangential stress may have been as high as 120 MPa–140 MPa. If we further assume relevant vertical stress ranges from about 1 MPa to 3 MPa from 50 m to 100 m overburden depths, and an elastic isotropic theoretical $\sigma_{max} = 3\sigma_H - \sigma_v$, we obtain estimates of σ_H of about 39 MPa–46 MPa. The implication is therefore that the ratio of principal stresses (σ_H/σ_v) may be as high as 20 or even 25, which of course is exceptional. In fact, the first visit to the power plant by the first author was to try to assess the reasons for an 80 m long crack close to the spillway exit (see Fig. 8).

A NNW-oriented horizontal stress was suspected, and the influence of a 'classic' lack of confinement close to the edge of the spillway gave all the conditions we have discussed for extensional-strain fracturing. The NNE regional stresses were concentrated in the ridge (due to river erosion?) and further concentrated by the perpendicular tunnelling. Stress (or extensional-strain) fracturing was worst when in the two most massive basalt flows. The stress

Fig. 8. Although this article has focused on extensional and shear modes of failure in initially intact massive rock, it is not forbidden to visualize the role of shear failure (and sometimes gravity-induced falls of rock) in creating serious stability problems. The examples illustrated are from Brazil and China. Three of the cases involve shear zones or faults, and tunnel excavation will have caused shearing and a worsening stability or actual tunnel collapse. The case with the yellow excavator illustrates the condition for 'inevitable' over-break, namely when the ratio $J_n/J_r \geq 6$ (Barton, 2007). Of course even when there are sufficient degrees of freedom for block fall-out (i.e. three joint sets: $J_n = 9$), the joint roughness J_r may cause too much dilation and prevent over-break. Also $J_n/J_r = 9/3$ is < 6 in this case, so no over-break occurs. Whether or not over-break occurs also depends on the frictional strength J_r/J_a, for instance in the case of the brown clay-coated feature (see bottom-left). Note the slickensides in this case.

Fig. 9. Stress-induced (or extensional-strain induced) fracturing and massive shear failure and rock burst effects in four TBM tunnels. It is our opinion that we may be observing the 'sharp' tip of log-spiral type shear failure in the two photographs on the left, in which medium strength marble and schist are involved, from China and Ecuador. Such was seen several times when inspecting a drained 11 km long headrace tunnel. The two right-hand photographs appear to show massive unstable shear failure, probably in the form of a moderate rock burst in the case of the marble, but less dynamic shearing/crushing in the case of the (5 MPa–10 MPa) chalk marl depicted in the 2.2 m diameter Beaumont Tunnel from 1880 (Bottom-right photo is from the UK Channel Tunnel area. This tunnel passed under a 70 m cliff).

(or extensional-strain) effect even fractured the basalt columns in the emergency spillway. This made the columnar basalt less resistant than usual to erosion from flood-flows. In effect, each basalt column was cracked in NNW directions (both vertically and horizontally) due to extensional strains. The estimated maximum horizontal stress of around 40 MPa was nowhere near high enough in relation to the UCS of about 200 MPa to cause 'compressive' failure (Barton and Infanti, 2003).

In TBM tunnels, it is easier to observe stress or strain induced fracturing. Due to the medium strength marble and schist shown in the left side of Fig. 9, it is believed that the tips of log-spiral shearing may be appearing instead of extensional-strain tensile fracturing. The massive failures on the right may be dynamic shearing and rock bursting (now covered in shotcrete), and in the case of the historic TBM tunnel (bottom-right) presumably a less violent shear-related crushing of this weak rock, which is less brittle than either the marble or the schist.

6. Mode 1 and mode 2 fracture modelling with FRACOD

We consider this section dealing with 2D fracture mechanics based modelling to be the logical conclusion concerning recommended modelling because various physically real mechanisms can be modelled, including extensional-strain induced (limited, initial) tensile failure, followed by coalescence of fractures and propagation in shear. The presence of joint sets and their 'disturbing' (reducing) effect on fracture propagation in shear can also be modelled (e.g. Fig. 10).

A number of FRACOD models have been used to investigate the mechanisms of tunnel spalling/failure. In all cases, an 8 m diameter tunnel was excavated, first of all, in an elastic and massive rock mass *without joints*. The in-situ stress state in the 2D plane perpendicular to the tunnel cross-section was assumed to be represented by a stress ratio of $\sigma_{Hmax}/\sigma_v = 2.0$, and a simulated depth of 1000 m was modelled in the first series of tests.

Model at 1000 m depth: Boundary stresses are $\sigma_{Hmax} = 50$ MPa and $\sigma_v = 25$ MPa. For the base case, the strength and fracture toughness of the rock were: UCS $\sigma_c = 165$ MPa; cohesion $c = 31$ MPa; internal friction angle $\phi = 49°$; tensile strength $\sigma_t = 14.8$ MPa. The mode I fracture toughness $K_{IC} = 3.8$ MPa m$^{1/2}$ and mode II fracture toughness $K_{IIC} = 4.7$ MPa m$^{1/2}$. The Poisson's ratio and Young's modulus are 0.24 and 68 GPa, respectively. (Note that all FRACOD models are for plane strain conditions).

The above parameters are the same as those of Äspö diorite, and are listed in the literature (e.g. Siren, 2012, who compares Finnish and Swedish rocks). The maximum tangential stress at the tunnel was calculated to be $\sigma_{max} = 150$ MPa, and the ratio of $\sigma_{max}/\sigma_c = 0.75$. Based on Martin et al. (1999), the depth of tunnel failure (from Fig. 3) is $R_f/a = 1.3$–1.5. For the case above, the predicted failure process is shown in progression in Fig. 11.

The key observations were:

(1) Fracture initiation occurred in the roof and floor where the compressive stress was the highest. The fracture initiation was driven by tensile strain due to the high compressive

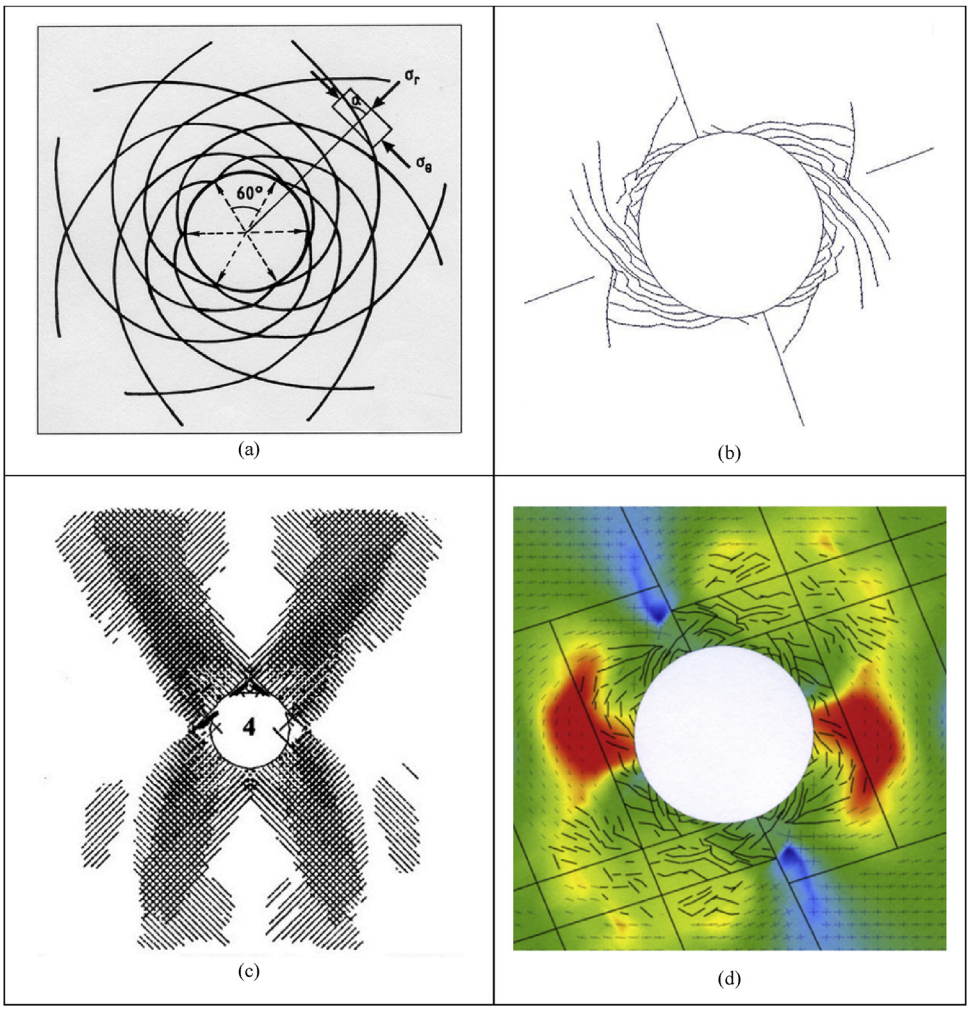

Fig. 10. From top-left, clockwise: (a) Log-spiral shear-failure analysis from Bray (1967a, 1967b). (b) An example of FRACOD modelling of a very deep (>2 km) TBM tunnel through the Peruvian Andes, with limited extensional-strain fracturing, so a quite 'pure' development of log-spiral shearing. Two perpendicular joints to represent massive rock cause little disturbance, as modelled. (c) A UDEC-MC model (Shen and Barton, 1997) to indicate the possible adverse effect of 'crushed rock' and ultra-deep EDZ in fault zones (10,000 blocks were modelled in this 'reducing block size' study). (d) FRACOD model with two joint sets of variable spacing. Most of the longer fractures are shear-driven and may represent the rock bursting effects often experienced at this project, with 2 m–3 m high voids resulting from ejected material above and ahead of the cutter-head.

stress, and the initiated fractures were sub-parallel to the tunnel wall surface.

(2) The new short fractures were not predicted to propagate in tension because there is no tensile stress in the tunnel wall. FRACOD predicts that they propagate in shear, forming a kink path from the initial fractures and they continue to propagate at an angle from the tunnel wall surface.

(3) As the propagation of the fractures near the tunnel wall progresses, new fractures continue to form deeper into the tunnel wall. These fractures also propagate in shear, eventually forming a larger (potential) break-out.

(4) The failure depth R_f/a is predicted to be 1.5, which is close to the upper limit predicted by Martin et al. (1999).

Overall, the modelling results indicate that fracture initiation forms due to extensional-strain related failure-in-tension mechanisms. However, the overall formation of the tunnel failure is predominately caused by shearing.

A number of cases were investigated by changing the fracture toughness K_{IIC} from 4.7 MPa m$^{1/2}$ to 11.5 MPa m$^{1/2}$ (The upper limit from the test data for Äspö diorite). There appears to be more tensile fracturing than the previous case with lower K_{IIC}. (Fractures marked in red are in tension; green are in shear). There were also many fracture sections sub-parallel to the tunnel wall. The predicted failure depth was $R_f/a = 1.25$, less than that of the previous case, but close to the lower limit of 1.3–1.5 from Martin et al. (1999) in Fig. 3.

In a further case, the mode II fracture toughness K_{IIC} was further increased from 11.5 MPa m$^{1/2}$ to 23 MPa m$^{1/2}$ (200% of the upper limit from the test data for Äspö diorite). In this case, only limited fracture initiation occurred. No fracture propagation and tunnel break-out were predicted. The predicted failure (damage) depth was now limited to $R_f/a = 1.1$, an unrealistically low value according to the case records assembled in Fig. 3 (and also incompatible with any need for an accelerated SRF value). So in preliminary conclusion, fracture initiation is predominately caused by tensile strain, whereas the (potential) break-out is formed by tensile (mode I) and shear (mode II) fracture propagation.

The modelling results suggest that a pure tensile mechanism for tunnel spalling and break-out is unlikely. The most likely mechanism is that the tunnel failure is caused by mixed tensile and shear, with shearing being the dominant mechanism. Higher K_{IIC} will encourage a greater tensile component in tunnel break-out. But if it is too high, no tunnel break-out is possible.

7. Combining FRACOD fracture mechanisms with dissipation by joint sets (1000 m)

Four models with joint sets were then modelled. The results are shown in Figs. 12 and 13. These models had the same (intact) rock mechanics properties as those shown in Fig. 11. Details of the jointing are listed below:

(1) One joint set with dip angle of 45° and spacing of 2.8 m.
(2) One joint set with dip angle of 45° and spacing of 1.4 m.
(3) Two orthogonal joint sets: dip angle of 45°, spacing of 2.8 m (Set 1) and 5.6 m (Set 2).
(4) Two orthogonal joint sets: dip angle of 45°, spacing of 1.4 m (Set 1) and 2.8 m (Set 2).

The mechanical properties of the joints were assumed to be: friction angle $\phi = 30°$; cohesion $c = 0$; dilation angle $\phi_d = 2°$; normal stiffness $K_n = 200$ GPa/m; shear stiffness $K_s = 20$ GPa/m. The simple linear Mohr-Coulomb failure criterion was used for the joint behaviour. The small dilation angle reflected the high stress levels at 1000 m depth.

The predicted fracturing patterns in the tunnel wall for the four jointed models are shown in Figs. 12 and 13 and the tabulated comments are given below each model, summarizing the differences between the models.

In summary, the introduction of joints to the model has led to less fracturing in the tunnel roof and floor, due presumably to the stress releasing effect of the jointing. The fracturing pattern is significantly affected by the joint geometry. The existence of joints did not change the overall fracturing mechanisms of the tunnel break-out, i.e. a mixed tensile and shear failure, with shear failure being the dominating cause. However the extent of the fracturing through intact rock (the actual need for fracturing) was obviously much reduced, as shear stresses could be dissipated to some extent by movement along the joints, which were quite weak. Rougher joints, with Barton JRC/JCS properties, and with Barton-Bandis scaling and non-linear effects, would be expected to have subtle effects, probably in the direction of more extensional and shear fracturing, as dilation would tend to reduce shearing along the joints, and reduce the shear stress dissipation.

8. Combining FRACOD fracture mechanisms with dissipation by joint sets at 2 km depth

Three additional models were run, one without joints and two with joints. The models have the same geometry as shown in Figs. 12 and 13, but the rock strength is reduced by 50% and the in-situ stresses are increased by 100% to simulate a tunnel in medium strong rock at a depth of 2 km. In very rough terms, we could suggest that this approximates the very challenging conditions

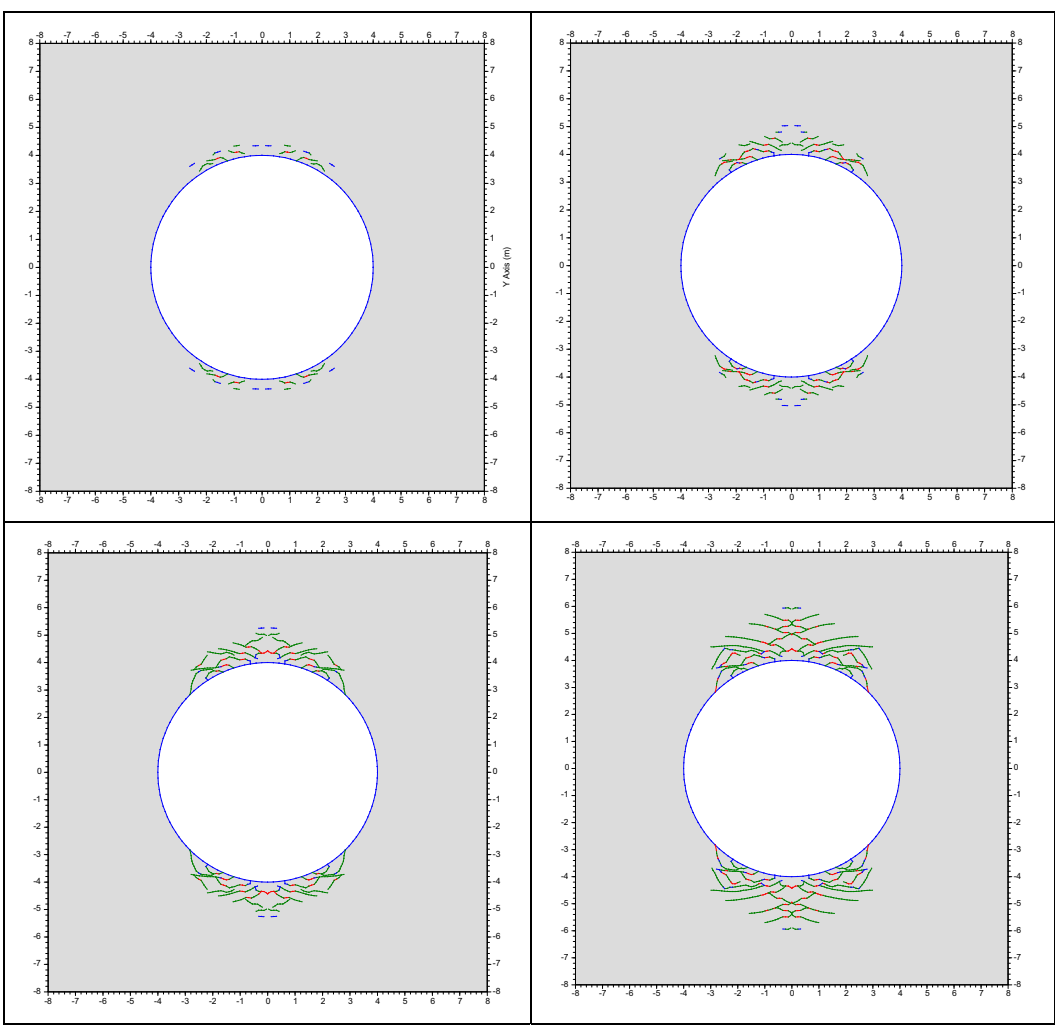

Fig. 11. A FRACOD model of a 1 km deep tunnel showing some of the progressive stages of fracturing, first due to the initial extensional-strain induced failure in tension (in red) despite the compressive stress field, followed by log-spiral style (and connecting) larger-scale shearing (in green).

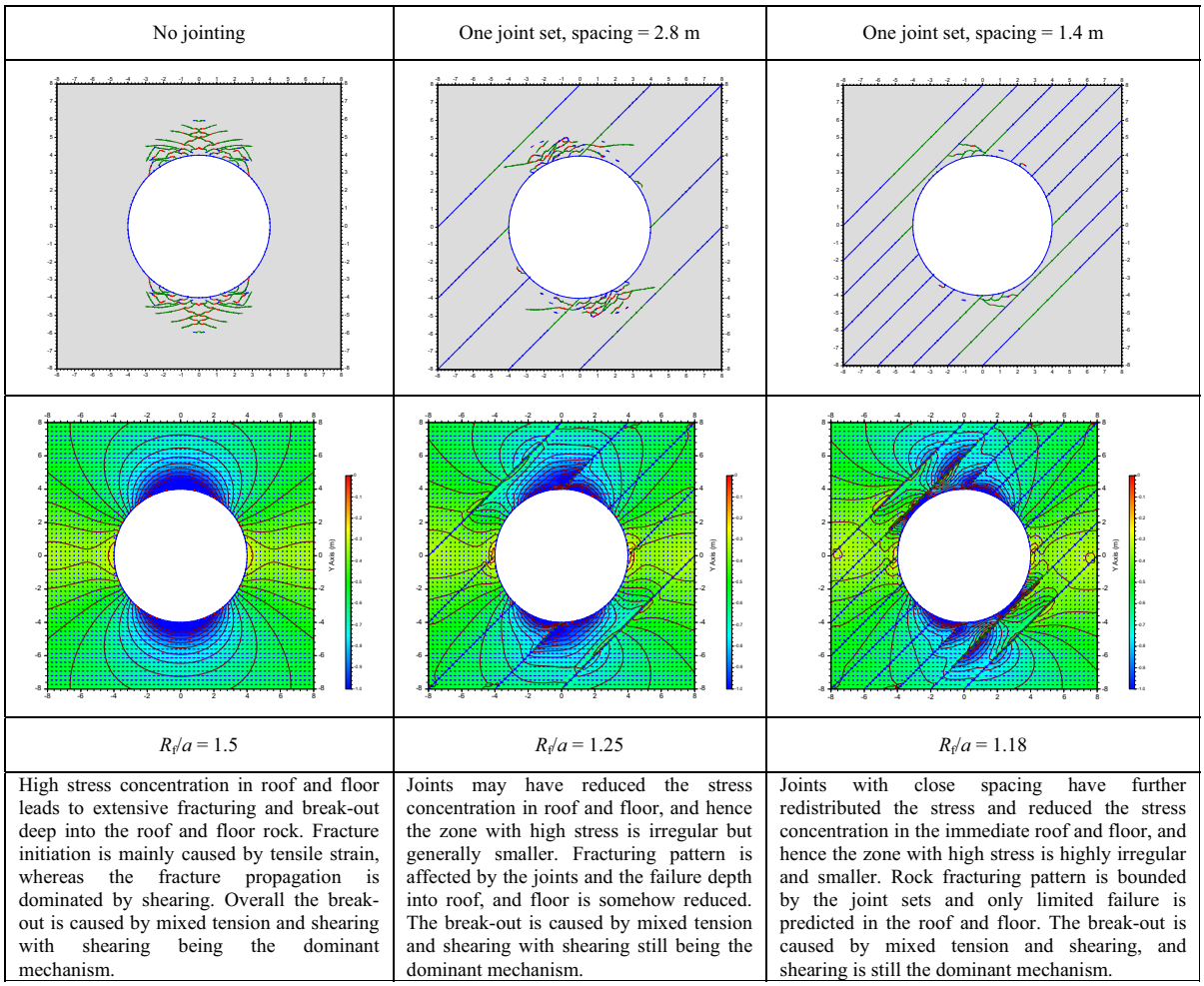

Fig. 12. FRACOD models of a 1 km deep tunnel. Comparison of fracturing behaviour when intact rock is replaced by *one set* of inclined joints, with two different spacings (2.8 m and 1.4 m). The development of the redistributed principal stresses is shown with blue contours. Shearing is evident, and hence the much reduced fracturing of intact rock, especially when the joints are more closely spaced. Note the strong reduction in R_f/a (Refer to Fig. 3).

inevitably experienced at Jinping II Project in China, where four 16.6 km headrace tunnels (plus transport and pilot tunnels) were driven through mountains giving an exceptional overburden depth of up to 2.5 km for several kilometres. However the horizontal stress is exaggerated, deliberately, in order to emphasize possible effects.

The added challenge, not presented in the Olmos Tunnel under the Andes (glimpsed in FRACOD models in Fig. 10), was that the predominantly marble rock-type had 'medium' strength (approximately 80–130 MPa) in comparison to the crystalline diorite (UCS, σ_c = 200 MPa) simulated in the first set of FRACOD models. Statistically speaking, when lower rock strength *also* occurs where there is higher stress, problems with potential rock bursts would be more likely.

Model at 2000 m depth. Boundary stresses assumed: σ_{Hmax} = 100 MPa and σ_v = 50 MPa. In this case, the strength and fracture toughness of the rock were: UCS σ_c = 82.5 MPa; cohesion c = 15.5 MPa; internal friction angle ϕ = 49°; tensile strength σ_t = 7.4 MPa, mode I fracture toughness K_{IC} = 1.9 MPa m$^{1/2}$; mode II fracture toughness K_{IIC} = 2.35 MPa m$^{1/2}$. Other input parameters such as the Poisson's ratio and Young's modulus are the same as those in the model of 1000 m depth. Please note that no attempt has been made to look for relevant Jinping II rock properties from the literature. This could be done in the future, combined with more realistic stress distributions. Note that high horizontal (tectonic) stress fields as modelled here, are a common feature of jointed, deep Western Australia mines. The model details are listed below:

(1) No joints (massive rock).
(2) One joint set with dip angle of 45° and spacing of 2.8 m.
(3) Two orthogonal joint sets, dip angle 45°, spacing 1.4 m (Set 1) and 2.8 m (Set 2).

The predicted failure patterns for the three models are shown in Fig. 14. For the model without joints, extensive fracturing occurred in the surrounding rock in the tunnel roof and floor. The failure depth showed $R_f/a > 1.5$ in the roof and floor. Nearly 70% of the tunnel surface was predicted to have extensive fracturing. The predicted fracturing was dominated by shearing. Laboratory experiments (e.g. Shen et al. (1995) indicate that shear fracturing in brittle materials tends to be very rapid and unstable). This is in contrast to tensile fracturing (e.g. wing cracks) under compression in which the crack growth is a stable and progressive process.

The extensive and shear-dominated fracturing in this model implies that, at the depth of 2 km with high tectonic stress, large tunnels in medium-strong rock masses are likely to experience dynamic and massive failure, which could be intense like a massive rock burst.

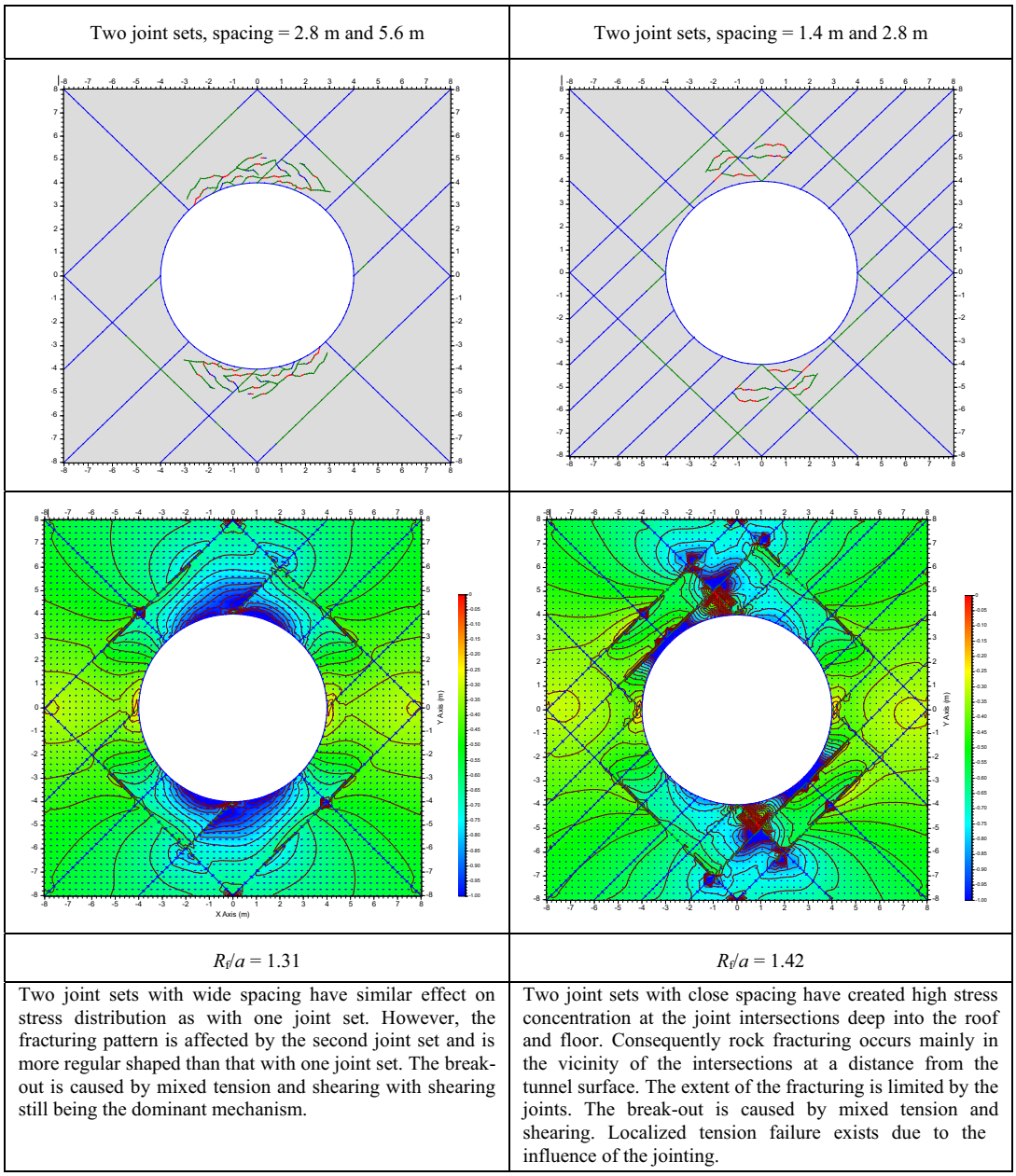

Fig. 13. FRACOD models of a 1 k m deep tunnel. Comparison of fracturing behaviour when intact rock is replaced by *two sets* of inclined joints, with two different spacings. The development of the redistributed principal stresses is shown with blue contours. Red contours indicate low compressive principal stress which occurs near the intersection of the joints due to stress redistribution. Shearing is evident, and hence the much reduced fracturing of intact rock, especially when the joints are more closely spaced. Note the strong reduction in R_f/a (Refer to Fig. 3).

The model with one joint set showed fracturing in the tunnel roof and floor extending more than 2 m into the rock. However, the depth of break-out (where intensive fracturing leads to near complete rock mass failure) was limited to about R_f/a of 1.25–1.38. The zone of fracturing at the tunnel wall was still fairly wide and covered more than 70% of the tunnel surface. Overall, compared to the model without joints, the predicted fracturing in the surrounding rock was somewhat reduced. Again this shows that the existence of joints has dissipated the shear stress concentration near the tunnel surface and hence reduced the (need for) rock fracturing.

In the case of the model with two joint sets at closer spacing, fracturing in the tunnel roof and floor was rather limited. Several new fractures occurred in the rock blocks in the roof and floor, but their propagation was terminated when meeting the existing joints. No clear wedge-shaped break-out was predicted from the limited rock fracturing. Numerous short fractures caused by fracture initiation appear in a wide range of the roof and floor, but these short fractures are not predicted to propagate to form rock failure. These fractures could be considered as a limited damage (rather than failure) in the intact rock. This model further demonstrates the effect of joints on tunnel break-out. Joints are playing a positive role in reducing the stress concentration and hence reducing the fracturing in the surrounding rock.

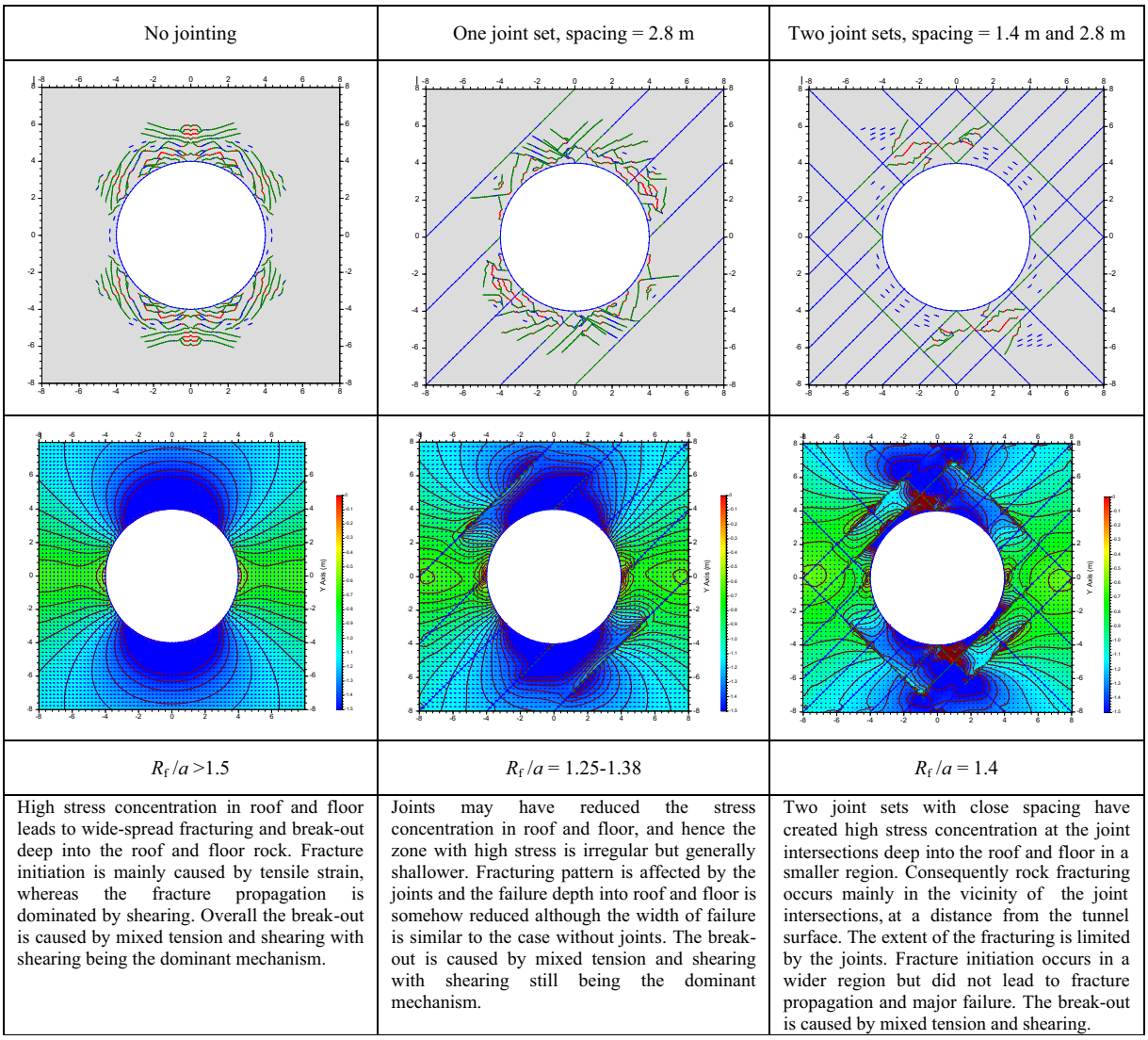

Fig. 14. FRACOD models of a 2 km deep tunnel. A comparison of fracturing behaviour when intact rock is replaced by one set, and then by two sets of inclined joints, with two different spacings (2.8 m and 1.4 m). The development of the redistributed principal stresses is shown with blue contours. Shearing is evident, and hence the much reduced fracturing of intact rock, especially when the joints are more closely spaced.

9. Discussion

Brittle failure of rocks is clearly dominated by explicit fracturing when the stresses are high enough, and when the rock is massive enough with sparse or very widely spaced jointing. This is different from the ductile failure that occurs when material yielding is more dominant. Rock mass failure criteria (such as the Mohr-Coulomb and Hoek-Brown criteria) based on the assumption of a continuum rock mass, may sometimes be adequate in predicting the zone of failure in the form of rock yielding, but are obviously at a disadvantage for describing explicit rock fracturing processes. Many recent studies (e.g. Hoek and Martin, 2014; Perras and Diederichs, 2016) continue to be carried out by modifying the continuum-based criteria, in order to better model brittle failure (such as tunnel spalling or break-out) with continuum modelling. Measures such as cohesion loss and friction mobilization have been used to produce results similar to observation. A nice example was shown in Fig. 6. This is one way (may be a complicated and inefficient way) of considering the failure initiation and propagation.

A rather different approach to failure initiation and propagation understanding is used in this paper. The fracture initiation and propagation during brittle failure are considered explicitly. A fracture mechanics-based numerical code developed by Shen et al. (2013), namely FRACOD, has been used as the tool for this investigation. Our FRACOD-based approach is rather different because of the actual modelling of fracture initiation and propagation, rather than the use of theoretical constitutive models and continuum modelling. Importantly, FRACOD also considers shear (mode II) fracture propagation which most traditional fracture mechanics approaches neglect.

The key advantage of the explicit fracturing approach is that it directly predicts the fracture initiation and the subsequent propagation under different stress conditions. We do not need to assume the failure mechanism (tensile or shear) or vary rock strength parameters during failure (such as strain-hardening or strain-softening). Rather, the formation of new fractures and their elongation (or propagation) will change the overall rock mass strength and other properties in the most realistic way, which is fully captured in the FRACOD approach.

As to the mechanism of tunnel failure, Hoek & Martin (2014) indicated *that shallow spalls are generally associated with pure tensile failure whereas deeper spalls are somewhat more complicated in that shear failure probably becomes involved as the notch tip moves away from the excavation boundary*. They also acknowledged that *numerical analyses of this failure process have proved to be extremely challenging and it has to be said that much work remains to be done before the complex interaction of tensile and shear processes associated with deep spall notches can be predicted with any degree of confidence*.

Our observation and modelling results indicate that pure tensile spalling is unlikely regardless of whether it is shallow spalling or deep spalling. Shear fracturing always plays a critical role in the failure process. It may be true that shallow spalling involves more tensile (or extensional-strain) fracturing than shear fracturing, but for deep spalling it is evident that shear fracturing is the dominant mechanism. It is possible that extensional-strain tensile fracturing cannot occur at great depth ahead of a tunnel. In this case log-spiral-type shearing may dominate to a greater extent. With the traditional continuum modelling approach, it is correctly stated by Hoek and Martin (2014) that it is an extremely challenging task to model the brittle spalling numerically. However, the explicit fracturing approach has been demonstrated to offer a new and promising way to study the tunnel spalling mechanisms at depth.

10. Conclusions

(1) Excavations in brittle rock, when at sufficient depth and in the absence of significant jointing, will tend to develop extensional-strain tensile fracturing close to the excavation, followed by coalescence and propagation of fracturing. The latter is dominated by shearing. The deeper the excavation is, the more dominant will be shearing, which is an unstable, dynamic, and possible rock bursting associated process. Both processes become limited when one or more joint sets are present, due to shear-stress dissipation on the joints, as opposed to the need for more stress-dissipating fracturing of intact rock, in order to gain equilibrium. So lack of jointing is a source of risk in deep hard-rock tunnels, whereas the presence of jointing can be a source of risk in shallow tunnels.

(2) The commonly occurring fracture-initiation stress/strength ratio of 0.4 ($\pm$0.1) representing the ratio of maximum tangential stress (estimated from linear elasticity: $3\sigma_1-\sigma_3$) and the uniaxial compression strength of the rock (σ_c or UCS), was noted in deep road tunnels in Norway, and marks the point when SRF accelerates in the Q-system, thereby providing more robust, risk-reducing tunnel or cavern support. Independently, fracture initiation and depth of failure have been related to increasing ratios of σ_{max}/σ_c in earlier case records from deep mining and from later Canadian URL break-out studies.

(3) The stress/strength ratio of 0.4 marking (extensional-strain-based) tensile fracture initiation, due to Poisson's ratio causing 'perpendicular' extensional tensile-fracturing, also marks the start of acoustic emission, both in the laboratory and in-situ. It turns out that the ratio 0.4, or close to this number, is a logical result of arithmetic. The arithmetic involves typical ratios of σ_c/σ_t (often about 10) and Poisson's ratio for (initially) intact rock (often about 0.25). The 'simplicity' behind the mysterious '0.4' was discovered by the second author when adding a new sub-routing to FRACOD. Stress/strength ratios beyond 0.4 represent a risk of extensional-strain-induced fracturing combined with the more hazardous shear fracturing, which may be associated with the risk of rock bursts.

Conflict of interest

The authors wish to confirm that there are no known conflicts of interest associated with this publication and there has been no significant financial support for this work that could have influenced its outcome.

References

Addis MA, Barton N, Bandis SC, Henry JP. Laboratory studies on the stability of vertical and deviated boreholes. In: Proceedings of the 65th SPE Annual Technical Conference and Exhibition of the Society of Petroleum Engineers. New Orleans: Society of Petroleum Engineers; 1990. p. 19–30. http://dx.doi.org/10.2118/20406-MS.

Barton N, Lien R, Lunde J. Engineering classification of rock masses for the design of tunnel support. Rock Mechanics and Rock Engineering 1974;6(4):189–236.

Barton N, Grimstad E. The Q-system following twenty years of application in NMT support selection. In: Proceedings of the 43rd Geomechanics Colloquy. Salzburg: Felsbau; 1994. p. 428–36.

Barton N. TBM Tunnelling in jointed and faulted Rock. Rotterdam: A.A. Balkema; 2000. p. 173.

Barton N. Some new Q-value correlations to assist in site characterization and tunnel design. International Journal of Rock Mechanics and Mining Sciences 2002;39:185–216.

Barton N. Failure around tunnels and boreholes and other problems in rock mechanics. Letter to ISRM News Journal 2003:12–8.

Barton N, Infanti N. Interpretation of exceptional stress levels from back-analysis of tunnelling problems in shallow basalts at the ITA Hydroelectric Power Project in S.E. Brazil. Tokyo: ARMS; 2003.

Barton N. Rock mass characterization for excavations in mining and civil engineering. In: Proceedings of International Workshop on Rock Mass Classification in Mining; 2007. p. 3–13. Vancouver.

Barton N, Pandey SK. Numerical modelling of two stoping methods in two Indian mines using degradation of c and mobilization of φ based on Q-parameters. International Journal of Rock Mechanics and Mining Sciences 2011;48(7):1095–112.

Barton N, Grimstad E. Q-system – an illustrated guide following 40 years in tunnelling, vol. 44; 2014. http://www.nickbarton.com/Downloads_New/2014.Barton-N-and_E-Grimstad_Q-system-an-illustrated-guide-following-40-years-in-tunnelling.zip.

Bieniawski ZT. Mechanism of brittle fracture of rock – part 1. Theory of the fracture process. International Journal of Rock Mechanics and Mining Sciences and Geomechanics Abstracts 1967;4(4):395–406.

Bray JW. A study of jointed and fractured rock. Part I. Fracture patterns and their failure characteristics. Felsmechanik 1967a;2–3:117–36.

Bray JW. A study of jointed and fractured rock. Part II. Theory of limiting equilibrium. Felsmechanik 1967b;4:197–216.

Brace WF. Brittle fracture of rocks. In: Judd W, editor. State of stress in the Earth's crust. New York: Elsevier; 1964. p. 111–80.

Brown ET, Trollope DH. The failure of linear brittle materials under effective tensile stress. Rock Mechanics and Engineering Geology 1967;5:229–41.

Fairhurst C, Cook NGW. The phenomenon of rock splitting parallel to the direction of maximum compression in the neighbourhood of a surface. In: Proceedings of the first Congress ISRM. Lisbon: ISRM; 1966. p. 687–92.

Grimstad E, Barton N. Updating the Q-system for NMT. In: Proceedings of International Symposium on Sprayed Concrete-Modern Use of Wet Mix Sprayed Concrete for Underground Support. Oslo: Norwegian Concrete Association; 1993. p. 20.

Gramberg J. Axial cleavage fracturing: a significant process in mining and geology. Engineering Geology 1965;1(1):31–72.

Hajiabdolmajid V, Martin CD, Kaiser PK. Modelling brittle failure. In: Girard J, Liebman M, Breeds C, Doe T, editors. Proceedings of the 4th North American Rock Mechanics Symposium, Seattle. Rotterdam: A.A. Balkema; 2000. p. 991–8.

Hoek E, Brown ET. Underground excavations in rock. London: Institution of Mining and Metallurgy; 1980. p. 527.

Hoek E, Martin CD. Fracture initiation and propagation in intact rock: a review. Journal of Rock Mechanics and Geotechnical Engineering 2014;6(4):287–300.

Martin CD, Chandler NA. The progressive fracture of Lac du Bonnet granite. International Journal of Rock Mechanics and Mining Sciences and Geomechanics Abstracts 1994;31(6):643–59.

Martin CD. Seventeenth Canadian Geotechnical Colloquium: the effect of cohesion loss and stress path on brittle rock strength. Canadian Geotechnical Journal 1997;34(5):698–725.

Martin CD, Kaiser PK, McCreath DR. Hoek–Brown parameters for predicting the-depth of brittle failure around tunnels. Canadian Geotechnical Journal 1999;36(1):136–51.

Müller L. The progressive failure in jointed media. In: Proceedings of ISRM Congress. Lisbon; 1966. p. 679–86 (in German).

Perras MA, Diederichs MS. Predicting excavation damage zone depths in brittle rocks. Journal of Rock Mechanics and Geotechnical Engineering 2016;8(1):60–74.

Read RS, Martin CD. Technical summary of AECL's Mine-by Experiment Phase 1: excavation response. Atomic Energy Canada Limited (AECL): Report AECL-11311, COG-95-171. 1996. p. 360.

Shen B, Stephansson O, Einstein HH, Ghahreman B. Coalescence of fractures under shear stresses in experiments. Journal of Geophysical Research Solid Earth 1995;100(B4):5975–90.
Shen B, Barton N. The disturbed zone around tunnels in jointed rock masses. International Journal of Rock Mechanics and Mining Sciences 1997;34(1):117–25.
Shen B, Stephansson O, Rinne M. Modelling rock fracturing processes: a fracture mechanics approach using FRACOD. Springer; 2013. p. 173.
Singh B, Jethwa JC, Dube AK, Singh B. Correlation between observed support pressure and rock mass quality. Tunnelling and Underground Space Technology 1992;7(1):59–74.
Siren T. Fracture toughness properties of rocks in Olkiluoto: laboratory measurements 2008–2009. Olkiluoto, Finland: Posiva Report 2012-25. 2012.
Stacey TR. A simple extension strain criterion for fracture of brittle rock. International Journal of Rock Mechanics and Mining Sciences and Geomechanics Abstracts 1981;18(6):469–74.
Stacey TR, Yathavan K. Examples of fracturing of rock at very low stress levels. In: Proceedings of the 10th ISRM Congress. Technology Roadmap for Rock Mechanics. Johannesburg, South Africa: SAIMM; 2003. p. 1155–9.
Wu H, Fang Q, Guo ZK. Zonal disintegration phenomenon in rock mass surrounding deep tunnels. Journal of China University of Mining and Technology 2008;18(2):187–93.

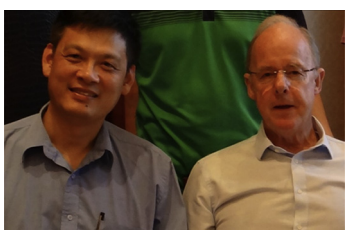

Dr. Nick Barton. Born in 1944, obtained a B.Sc. in Civil Engineering from King's College in 1966, and a Ph.D. concerning shear strength and rock slope stability from Imperial College in 1971. He has worked 25 years at NGI in Oslo and 4 years at TerraTek in Salt Lake City. Since 2000 he has had his own international rock engineering consultancy, Nick Barton & Associates, based in Oslo and São Paulo. He has consulted on hundreds of rock engineering projects in a total of 38 countries during 45 years, has 260 publications as first or single author, and has written two books, one on TBM prognosis, the other linking rock quality and seismic attributes of rock masses at all scales. He is currently writing a book with Stavros Bandis: *Engineering in Jointed and Faulted Rock* (expected late 2017). He has ten international awards including the 6th Müller Lecture of ISRM. He developed the widely used Q-system for classifying rock masses, and for selecting rock tunnel and cavern single-shell support in 1974. He was originator of the rock joint shear strength parameters JRC and JCS and co-developer of the resulting Barton-Bandis constitutive laws for rock joint modelling in 1982, which was incorporated as a sub-routine in UDEC-BB in 1985. He also developed the Q_{tbm} prognosis method and Q_{slope} for selecting maintenance-free rock slope bench-face angles. His chief areas of consulting activity have been in hydropower tunnelling and cavern construction, nuclear waste disposal site characterization, metro tunnels and caverns, and site characterization at high dams. He has given more than thirty five keynote lectures in international conferences.

Dr. Baotang Shen. Born in 1964, presently Senior Principal Research Scientist and Group Leader at CSIRO, Brisbane, Australia, and Adjunct Professor at Shandong University of Science and Technology, China. He graduated from the Department of Mining Engineering, Northeastern University in 1985; Obtained Ph.D. from Royal Institute of Technology (KTH), Sweden in 1993; Visiting Scholar at Massachusetts Institute of Technology (MIT) in 1993; Postdoc Research Fellow at Norwegian Geotechnical Institute (NGI) in 1994. Since 1995 he has been working with the Commonwealth Scientific and Industrial Research Organisation (CSIRO), Australia. Dr. Shen's main research areas are: Rock mechanics, Rock fracture mechanics; Deep mining engineering, Mining environmental engineering. He is currently a member of Australia Standard Committee of Geotechnical Investigation, a reviewer of many leading international journals such as *International Journal of Rock Mechanics and Mining Sciences*, *Rock Mechanics and Rock Engineering*, etc. Dr. Shen has recently been leading the following major research projects: "International Collaboration Project on Coupled Fracture Mechanics Modelling"; "Remediation of Abandoned Old Mines" supported by Queensland State Government; "Overburden Grout Injection Technology to Prevent Mine Subsidence" supported by BHP Billiton; "Roof fall Monitoring and Early Warning Technology" supported by JCOAL; "Integrated Coal and Gas Extraction for Deep Mines – Field Monitoring" – supported by Huainan Coal Mine Group. Dr. Shen has published one book "Modelling Rock Fracturing Processes", more than 110 papers in journals and conference proceedings, and about 50 technical reports.